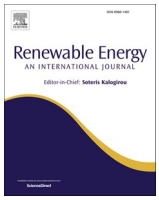
Renewable Energy 259 (2026) 124936



Contents lists available at ScienceDirect

Renewable Energy

journal homepage: www.elsevier.com/locate/renene



Integration of energy storage systems with adjustable curtailment of photovoltaic generation in power distribution networks for enhanced grid efficiency

Pradeep Ammasaikutti [a,*], Alex Stanley Raja Thaveedhu [b], Muruganantham Jayapalan [a], Kannan Palanisamy [c]

[a] Department of Electrical and Electronics Engineering, Vivekanandha College of Engineering for Women, Elayampalayam, Tiruchengode, Namakkal, Tamilnadu, India
[b] Department of Electrical and Electronics Engineering, Bannari Amman Institute of Technology, Sathyamangalam, Erode, Tamilnadu, India
[c] Department of Electrical and Electronics Engineering, Angel College of Engineering and Technology, Pollikalipalayam, Tiruppur, Tamil Nadu, India

ARTICLE INFO

Keywords:
Photovoltaic generation
Energy storage systems
Energy management
Load demand prediction
Cost reduction

ABSTRACT

Although renewable energy sources can produce electricity efficiently, there are certain operational challenges when integrating them into the power grid. To mitigate these issues, this manuscript proposes a new approach for integrating Energy Storage Systems (ESS) with adjustable curtailment of photovoltaic generation in power distribution networks to develop grid efficiency, reduce energy costs, and improve system reliability. The proposed technique involves the Logarithmic Differential Convolutional Neural Network (LDCNN) and Eel and Grouper Optimizer (EGO) technique, which is commonly referred to as LDCNN-EGO. The objective is to improve grid efficiency and reduce costs and enhance system reliability. The LDCNN method is used to predict the load demand, and the EGO is used to optimize the locations and size of ESS in power distribution networks. The proposed method is implemented using MATLAB to evaluate its performances and compared with the existing methods like sizing algorithms (SA), Coot Bird Search Algorithm-Genetic Algorithm (CBSA) and Crayfish Optimization Algorithm (COA). The proposed method attains the lowest operational cost of $27.2, outperforming SA ($28.3), CBSA ($29.3), and COA ($30.3). This approach effectively improves grid reliability while supporting a smoother transition toward a sustainable energy system.

1. Introduction

1.1. Motivation and incitement

The increasing combination of photovoltaic (PV) systems into power distribution grids is driven by their crucial role in achieving fossil-free energy transition targets [1]. As PV generation capacity expands, distribution grids are expected to handle substantial levels of PV output in the future [2]. However, this growth introduces challenges such as voltage limit violations, line congestion, and substation transformer overloading, particularly when PV generation exceeds nominal demand [3]. These issues can compromise grid stability and efficiency, necessitating effective solutions [4]. Energy storage systems (ESSs) offer a promising solution by storing excess PV generation through low-demand periods and supplying energy when required [5]. ESSs help balance generation and consumption, minimize grid instability, and prevent energy curtailment during peak generation times [6,7]. By reducing strain on distribution infrastructure, ESSs mitigate overloading and congestion issues, enhancing grid flexibility and reliability [8,9]. As the energy transition accelerates, ESSs become essential for supporting large-scale PV integration into power distribution networks [10].

A key challenge in grid planning is the simultaneous consideration of grid constraints and PV curtailment when sizing and placing ESSs. Many existing methods overlook these constraints or fail to integrate them with optimal ESS allocation. Modeling nodal voltages, line capacities, and transformer limits is complex, especially with non-linear power flow, and traditional AC optimal power flow methods are computationally intensive, highlighting the need for efficient ESS placement and sizing strategies in PV-dominated networks.

* Corresponding author.
E-mail addresses: cruisepradeep@gmail.com (P. Ammasaikutti), alexstanleyraja@gmail.com (A. Stanley Raja Thaveedhu), murugananthamj82@gmail.com (M. Jayapalan), pkannannkl@gmail.com (K. Palanisamy).

https://doi.org/10.1016/j.renene.2025.124936
Received 30 June 2025; Received in revised form 10 October 2025; Accepted 1 December 2025
Available online 3 December 2025
0960-1481/© 2025 Published by Elsevier Ltd.

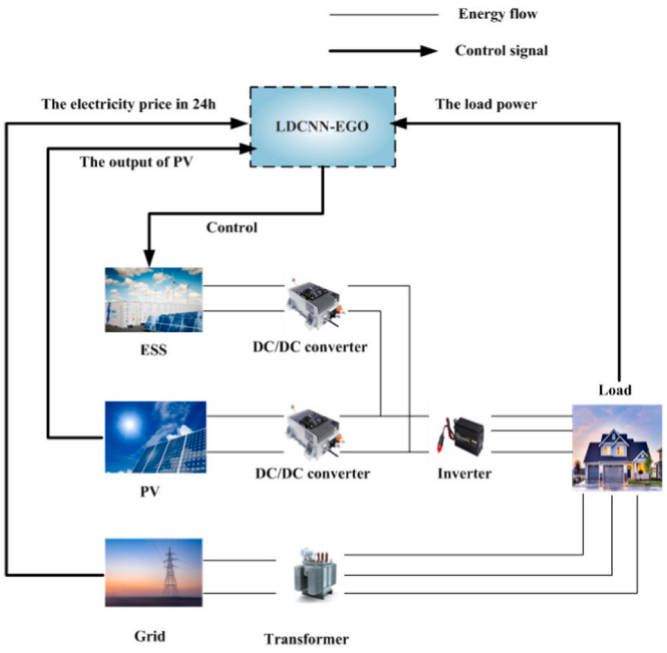


Fig. 1. Structure of energy storage system with proposed approach.

1.2. Literature review

Several research works presented in the literature were based on PV-based energy storage systems; a few of them were reviewed here, Bhol and Sahu [11], implemented optimal scheduling of a microgrid integrating PV and battery storage using a crayfish optimization algorithm. The methodology employed MATLAB Simulink to manage multiple renewable sources, addressing economic dispatch and uncertainty in energy management. The approach enhanced operational efficiency and cost management, demonstrating improved handling of energy flow in grid-connected microgrids. Limitations included potential challenges in scalability to larger microgrids and adapting to highly variable environmental conditions.

Borkowski et al., [12] have presented a grid-connected photovoltaic farm's battery energy storage system (BESS), with an emphasis on energy management and sizing algorithm (SA). The methodology combined a dedicated PV energy management strategy with bidirectional energy transfer to maximize daily market revenue and optimize financial criteria. The approach enhanced profitability and operational efficiency, though its reliance on complete PV production and price data and limited adaptability to varying market conditions posed notable limitations.

Memarzadeh and Keynia [13], applied MRMI-Long Short-Term Memory (LSTM) forecasting combined with Coot Bird Search Algorithm-Genetic Algorithm (CBSA) optimization to plan PV and energy storage systems in distribution networks. The methodology used feature selection and LSTM predictions to determine optimal sizes and locations, aiming to reduce voltage deviations, power losses, and costs. The approach enhanced system performance and efficiency, while high computational complexity and implementation challenges remained limitations.

Zhang et al., [14] applied intelligent reinforcement learning to optimize energy storage operation in photovoltaic-storage charging stations. The methodology modeled efficiency and capacity degradation, using a dual delay deterministic strategy gradient to manage charging and discharging under uncertain PV output, EV demand, and electricity prices. The approach improved operational efficiency and revenue, while high training and computational complexity remained a limitation.

Abdelsattar et al., [15] evaluated multiple machine learning (ML) algorithms for predicting photovoltaic energy in sustainable systems. The methodology compared Categorical Boosting (CatBoost), Multilayer Perceptron (MLP), Gradient Boosting Machine (GBM), Support Vector Machine (SVM), Xtreme Gradient Boosting (XGBoost), and Random Forest using extensive solar generation data, assessing consistency and accuracy. The approach enhanced forecast precision and reliability, particularly through XGBoost and Random Forest, while some models struggled to generalize to unseen data.

Shabbir et al., [16] applied deep learning (DL) driven PV forecasting and battery management to develop PV hosting capacity and mitigate congestion in distribution networks. The methodology employed LSTM for day-ahead PV prediction to control residential battery energy storage systems, reducing overvoltage and line overloading. The approach strengthened network reliability and economic efficiency, though its effectiveness depended on accurate load and PV data, and high computational requirements posed additional limitations.

Karthikeyan and Manimegalai [17], investigated power control in hybrid grid-connected renewable energy systems integrating solar, wind, and battery storage. The methodology combined genetic algorithms with a nested ML framework, including TD Lambda learning, to optimize battery health, discharge-charge cycles, and energy costs while maintaining 24-h load demand. The approach enhanced operational efficiency and cost-effectiveness, though high computational complexity and dependency on accurate system parameters limited broader applicability.

Ganesh et al., [18] applied an optimized Extreme Learning Machine (ELM) for short-term forecasting of photovoltaic generation to manage energy storage in grid-connected systems. The methodology used forecasted and measured power to control charging and discharging via a DC–DC bidirectional converter. The approach enhanced grid stability and energy balance, though reliance on accurate environmental data and model tuning posed limitations for wider deployment.

Previous studies emphasize the role of optimization and machine learning (ML) in improving Energy Storage Systems (ESS) and Photovoltaic Generation for efficient grid operation. The COA often suffers from slow convergence and susceptibility to local optima, while SA becomes computationally expensive for large-scale networks and lacks adaptability to dynamic conditions. The CBSA tends to require high computational resources and face premature convergence issues. The Dual Delay Deterministic Gradient Algorithm is unstable in highly nonlinear conditions and shows sensitivity to delay factors. SVMs struggle with scalability and increased training complexity as problem size grows. LSTM networks demand significant computational resources and have high training times. Genetic Algorithms (GA) face challenges with slow convergence and maintaining solution diversity. ELM, while fast, generally offers limited robustness and reduced accuracy in handling intricate system dynamics. These challenges motivate the need for an integrated and efficient framework capable of optimizing energy storage deployment and PV generation while ensuring reliability and computational efficiency, forming the basis for the proposed LDCNN-EGO method.

1.3. Contributions and paper organization

To address the limitations identified in the literature, this study introduces the LDCNN-EGO framework. The proposed LDCNN-EGO framework integrates deep learning-based forecasting with intelligent optimization to enhance overall grid performance. The LDCNN efficiently models complex nonlinear and dynamic behaviors using logarithmic differential activation, which ensures faster convergence, improved feature extraction, and higher forecasting accuracy. In parallel, the EGO enhances global search efficiency, maintains solution diversity, and avoids premature stagnation through a balanced exploration-exploitation mechanism. The LDCNN-EGO framework achieves robust, scalable, and adaptive energy management with reduced computational complexity, improved stability, and reliable operation

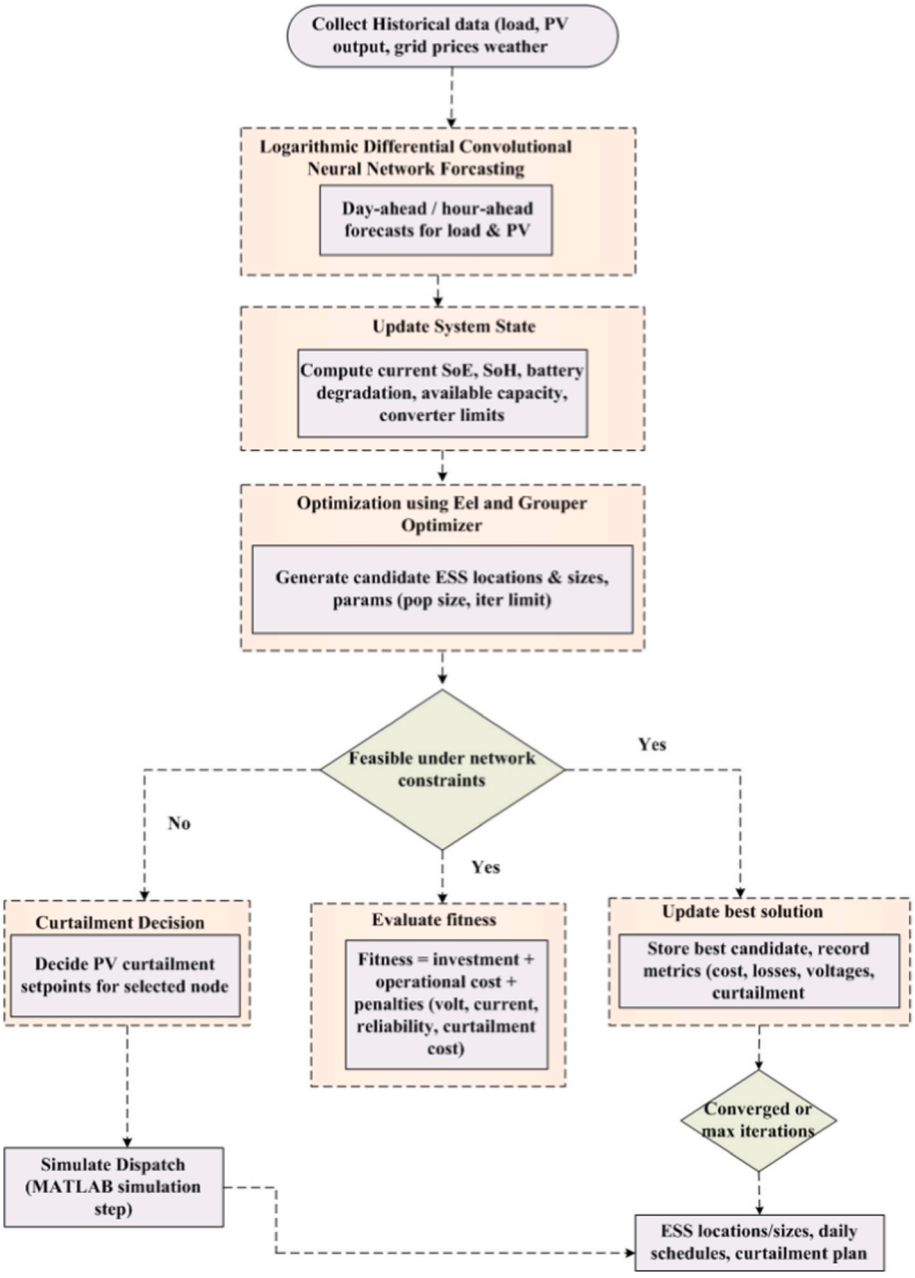


Fig. 2. Flowchart of the proposed PV-ESS management strategy.

under varying grid conditions.

The following list lists the important contributions made by this paper.

- Proposes an integrated LDCNN-EGO framework that jointly optimizes ESS management and PV curtailment to enhance grid efficiency and minimize operational costs.
- Introduces LDCNN for nonlinear load prediction and dynamic forecasting, ensuring faster convergence and higher feature extraction accuracy.
- Employs EGO to achieve robust global optimization, balancing exploration and exploitation while avoiding premature stagnation.
- Demonstrates superior adaptability and scalability in handling large-scale, dynamic grid environments with reduced computational complexity.
- Provides a comprehensive strategy that enhances grid stability, energy utilization, and reliability under varying demand and supply conditions.

The balance manuscript is as follows: sector 2 gives the configuration of the microgrid system for optimized energy management, sector 3 discusses the proposed LDCNN-EGO approach, sector 4 shows the results and discussions and sector 5 concludes the research.

2. Configuration of power distribution for optimized energy management system

Fig. 1 shows that the structure of energy storage systems with proposed approach. The proposed system model represents a microgrid that integrates renewable energy sources, specifically PV panels, with an ESS and a connection to the main grid. The system uses DC/DC converters and inverters to convert and manage energy flows between the

renewable energy sources. An optimization algorithm governs the system, dynamically adjusting the discharging and charging of the ESS, reducing the output of the PV generation when there is excess power or grid constraints, and determining the optimal power exchange with the grid. The primary goal of the system is to maximize the use of renewable energy, store excess energy in the ESS for later use, and minimize operating costs through efficient energy management. This approach ensures grid stability, reduces reliance on the grid, and optimizes overall energy efficiency, contributing to both economic and environmental benefits. Fig. 2 shows the flowchart of the proposed PV-ESS management strategy.

2.1. Energy storage system

The degree of battery aging over time is quantified using the State of Health (SoH), defined as [19]:

$$SOH = 1 - \frac{Q_{loss,t}}{Q_{rated}} \tag{1}$$

where, $Q_{loss,t}$ indicated as the capacity lost at time t (MWh), Q_{rated} is the initial battery capacity (MWh). SoH provides a measure of battery life degradation at different moments during operation. The battery's cycle aging depends on both the **cycle depth** h and the **number of cycles** n. To integrate cycle aging into optimization, the general degradation relation is transformed into a single-cycle formulation:

$$Q_{cycle}(h) = A \exp\left(\frac{-E_a}{RT}\right)(hE_{rate})^z \tag{2}$$

where, $Q_{cycle}(h)$ represents the capacity degradation per cycle, and the other parameters describe material properties and operating conditions. The model assumes that cycle aging occurs primarily during the discharging stage, as the energy change between charge and discharge is nearly identical. The cycle depth during discharge is expressed as:

$$h_t = \frac{1}{\eta dis E_{rate}} P_{dis,t} \Delta t \tag{3}$$

where, $P_{dis,t}$ is denoted as the discharging power (MW), ηdis is indicated as the battery discharge efficiency (%), h_t is denoted as the cycle depth at time t. This formulation allows the optimization model to account for **battery efficiency, cycle depth, and degradation** when scheduling charge and discharge operations.

2.2. PV modelling

Equation (2) is used to calculate the PV panel's power generation, or $P_{PV}(kW)$.

$$P_{PV} = \tau \times I_{AM} \times I_T \times \eta_{PV} \times CAP_{PV} \tag{4}$$

The PV cover material's combined incidence angle modifier, or I_{AM}, ranges from 0 to 1, The sum of the solar radiation that strikes the PV collect surface is known as $I_T(W/m^2)$, the PV array's overall efficiency is called η_{PV}, the PV surface area is called $CAP_{PV}(m^2)$. At a normal incidence angle, the transmittance, absorptance, and product of solar radiation on the PV cover is known as τ.

2.3. Grid modeling

The grid utility can trade electricity based on the availability of renewable energy sources, like excess or insufficient energy produced. In general, purchasing electricity from the grid at a time when prices are high is not a good way to reduce electricity costs. Time-of-use, fixed price, and real-time price are some of the many methods for determining electricity prices.

The grid utility's exchange power at time t is denoted as $P_g(t)$ kW and may be computed as follows:

$$P_g(t) = L(t) - P_{sT}(t) - P_{wT}(t) + u(t) \tag{5}$$

under the following circumstances:

$P_g(t) > 0$ If power is taken from the grid, and

$P_g(t) < 0$ if power is exports to the grid.

Where $P_{sT}(t)$ is denoted as total solar power at moment t, $P_{wT}(t)$ is indicated as total wind power at time t, $L(t)$ is denoted as load at time t, and $P_g(t)$ is denoted as grid power at time t.

2.4. Objective function

The aim is to discover the most cost-effective locations and dimensions for energy storage systems in a distribution network that connects to distributed PV generation, prosumers, and electrical demand. While taking into account optional PV curtailment, minimizing investment and operating costs, and accounting for electricity consumption and PV energy sales revenues, it seeks to meet the grid's operational constraints.

2.4.1. Cost function

2.4.1.1. Investment costs for ESSs. Let $E_n^{ess} \in R^+$ and $P_n^{ess} \in R^+$ represent, respectively, the rated power of the ESS's converter and its energy capacity at the node. The binary variable $F_n^{ess} \in \{0,1\}$ indicates whether the ESS is set up at the node n. The cost of installing an ESS with a power rating P_n^{ess} and energy capacity E_n^{ess} is as follows [20]:

$$J^I\left(P_n^{ess}, E_n^{ess}, F_n^{ess}\right) = C^P P_n^{ess} + C^E E_n^{ess} + C^F F_n^{ess} \tag{6}$$

here C^P, C^E, and C^F stand for the unitary costs of installation, energy capacity, and rated power, respectively.

2.4.1.2. Operational costs. The grid operator purchases and sells electricity to pay for energy storage's operating expenses.

$$J_{n,t}^{O\ P} = P_{n,t}^{im} c_t^{im} - P_{n,t}^{ex} c_t^{ex} \tag{7}$$

where c_t^{im} denote as Grid electricity purchased, c_t^{ex} denote as Electricity sold wholesale, $P_{n,t}^{im}$ and $P_{n,t}^{ex}$ be node n's and time t's nodal imported and exported power.

The objective function is:

$$OB = A \times J^I\left(P_n^{ess}, E_n^{ess}, F_n^{ess}\right) + B \times J_{n,t}^{OP} \tag{8}$$

where A and B are the weighting parameters and $J^I\left(P_n^{ess}, E_n^{ess}, F_n^{ess}\right)$ is denoted as the investment cost and $J_{n,t}^{OP}$ denote as operational cost.

2.4.2. Constraints

2.4.2.1. Grid. With grid constraints represented by a linearized sensitivity coefficient method, in situations where the load flow is locally invertible, a unique solution is ensured by modeling a balanced three-phase system using a single-phase equivalent. Both an active and a reactive nodal injection are simultaneously displayed in equation (9).

$$P_t = P_t^{pv} - P_t^{load} - P_t^{ess} \tag{9}$$

$$q_t = q_t^{pv} - q_t^{load} - q_t^{ess} \tag{10}$$

where P_t^{pv}, P_t^{load}, P_t^{ess} and q_t^{pv}, q_t^{load}, q_t^{ess} collect aggregated reactive and active power injections of PV power, ESS power, and load, correspondingly.

2.4.2.2. Constraints of PV generation. PV generation potential is modeled based on the local plane-of-array irradiance, adjusted for plant

Table 1
Parameter table for LDCNN.

Parameter	Values
Convolutional Layers	2 -5 layers
Filter Size	3 × 3, 5 × 5, 7 × 7
Activation Function	Logarithmic Differential Activation
Pooling Strategy	Max Pooling, Average Pooling
Learning Rate	0.001
Batch size	32
Dropout Rate	0.5

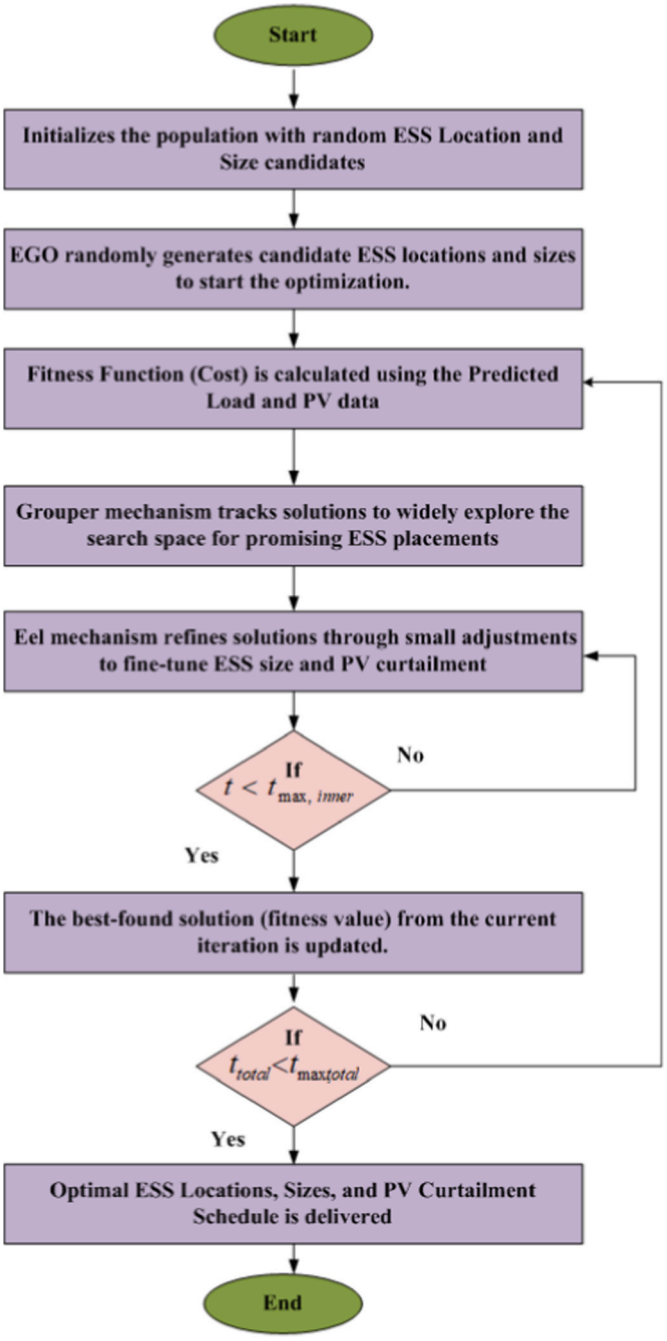


Fig. 3. Flowchart of ego

rated power and temperature. The PV generation potential $\widehat{p}_{n,t}^{pv}$ for a plant with rated power p_n^{pv} is:

$$\widehat{p}_{n,t}^{pv} = I_t\left[1+\alpha\left(T_t^{air}+\beta I_t-25\right)\right]p_n^{pv} \tag{11}$$

here T_t^{air} denote as air temperature, I_t denote as POA irradiance, $\alpha = -0.0043$ and $\beta = 0.038$ are measurements for open-rack photovoltaic plants.

2.4.2.3. Constraints of ESS operations. Injections of controlled active and reactive power $P_{n,j}^{ess}$ and $q_{n,t}^{ess}$, which are contingent upon the converter's energy requirements and capability curve, are used to depict ESS operations. The first restriction is as follows:

$$0 \le \left(P_{n,j}^{ess}\right)^2 + \left(q_{n,j}^{ess}\right)^2 \le \left(P_n^{ess}\right)^2 \tag{12}$$

The linearity of the constraints is preserved by approximating this convex expression using a piecewise linearization technique. In order to accurately depict energy dynamics over the operational horizon, a time-dependent function is used to model the evolution of the ESS's state-of-energy (SOE).

$$SOE_{n,j+1} = SOE_{n,j} - P_{n,j}^{ess}\Delta t \tag{13}$$

where, Δt is the sampling time. The SOE is maintained within safe operating limits defined by:

$$aE_{ess,n} \le SOE_{n,t} \le 1-a$$

with $0 \le a \le 0.50$ as an adjustable parameter and $E_{ess,n}$ representing the ESS energy capacity. Virtual gearbox lines are added to the load flow problem to account for the ESS's charging and discharging losses, represented via an equivalent resistance R_{ess}. The resistance is iteratively updated based on the ESS's power and energy capacities, which are decision variables in the optimization problem, and this method replicates the ESS losses without the use of binary variables. The initial expression for the ESS equivalent resistance in per-unit (p.u.) is:

$$R_{ess} = \frac{E_{ess}^{loss}}{\sum_\tau \left(P_{ess,t}\right)^2 \Delta t} \tag{14}$$

where, E_{ess}^{loss} represents the total losses of the ESS, Taking into account that the resistance-based and efficiency-based models are equivalent, the losses can be expressed as $E_{ess}^{loss} = \eta E_{ess}$,where η is denoted asthe efficiency obtained from ESS and converter datasheets. Substituting this, the resistance becomes:

$$R_{ess} = \frac{\eta E_{ess}^{loss}}{\sum_\tau \left(P_{ess,t}\right)^2 \Delta t} \tag{15}$$

For computing a resistance valid under worst-case conditions when the ESS operates mostly at full power the instantaneous power $P_{ess,t}$ is replaced with the rated power P_{ess}. Under this assumption, the resistance is given by:

$$R_{ess} = \frac{\mu E_{ess}^{loss}}{\sum_\tau \left(P_{ess,t}\right)^2 \Delta t} = R_{ess} = \frac{E_{ess}^{loss}}{\sum_\tau \left(P_{ess,t}\right)^2} \tag{16}$$

where, $R_{ess0,}$ is a constant derived from the manufacturer's datasheet. This formulation makes it evident that the ESS resistance is inversely proportional to the converter's power rating and proportional to the energy capacity. As a result, throughout every planning optimization iteration, the ESS resistance is updated according to (16) as the energy and power sizes are adjusted.

2.4.2.4. ESS installation variables. The binary variables $F_{ess,n}$ indicate whether an ESS is installed at the node n and are linked to the corresponding energy capacity and converter power rating as follows:

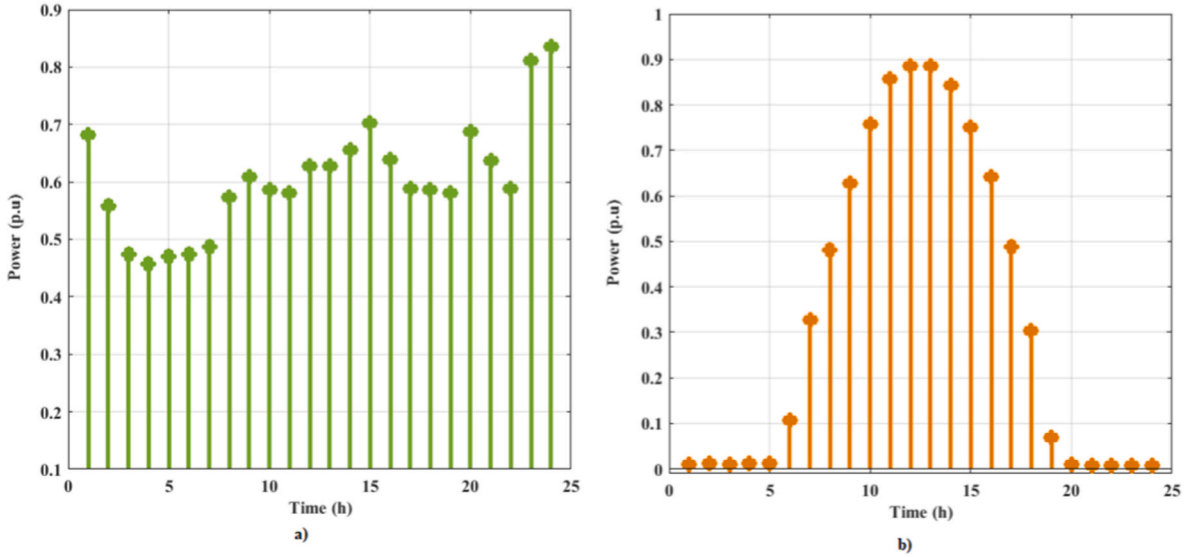


Fig. 4. Analysis of the reduced scenario set for the sizing simulation: (a) Load scenarios and (b) Global Horizontal Irradiance (GHI) scenarios.

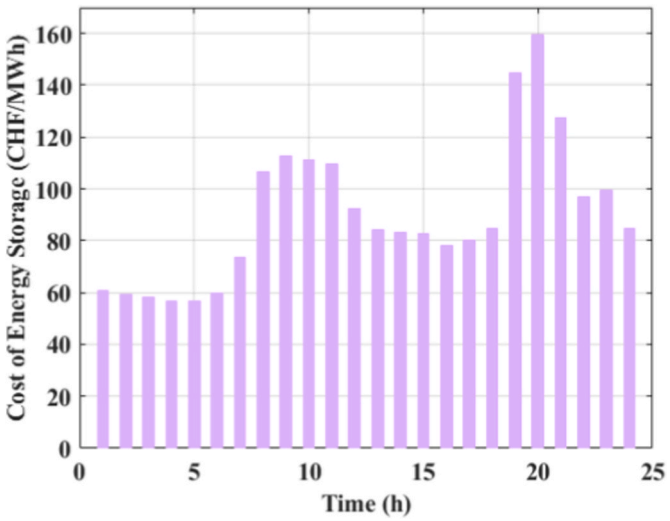


Fig. 5. Analysis the typical price trends.

$$F_{ess,n}P_{ess,n}^{\min} \le P_{ess,n} \le F_{ess,n}P_{ess,n}^{\min} \tag{17}$$

$$F_{ess,n}E_{ess,n}^{\min} \le E_{ess,n} \le F_{ess,n}E_{ess,n}^{\min} \tag{18}$$

where, $E_{ess,n}^{\min/\max}$ and $P_{ess,n}^{\min/\max}$ are customizable parameters that define the allowable ranges of energy capacity and power rating, which can be adjusted based on practical considerations such as space availability or land-use constraints.

2.5. Formulation of the planning problem

The installation locations, power ratings, energy capacities, and charge/discharge profiles of the ESS units, as well as PV production levels modified for curtailment at every distribution network node, are the decision variables in the ESS planning problem. The set contains a collection of these variables:

$$\chi = \left\{P_{ess,n}, E_n^{ess} \in \Re^+, F_n^{ess} \in +\{0,1\} p_{pv,n,t}, p_{ess,n,t}, q_{ess,n,t} \forall n \in N, t \in T\right\}$$

Considering a planning horizon of n_y years, the objective of the ESS planning problem is to minimize the total investment and operational costs, formulated as:

$$\min_{\chi} \sum_{n\in N} J_I\left(P_{ess,n}, E_n^{ess}, F_n^{ess}\right) + \sum_{y=1}^{n_y} \sum_{t\in T} \sum_{n\in N} J_{n,t}^{OP}\left(P_{n,t}^{pv}, P_{n,t}^{ess}\right) \tag{19}$$

The ESS planning problem defined in (19) aims to optimally determine the locations, capacities, and operational schedules of energy storage systems while coordinating PV curtailment, such that the total investment and operational costs over the planning horizon are minimized. This formulation ensures that both technical constraints of the grid and operational limits of ESS and PV units are respected, providing a cost-effective and reliable strategy for integrating distributed energy resources into the distribution network.

3. Proposed LDCNN-EGO optimizes ESS with curtailment of photovoltaic (PV) generation

In this section, proposed LDCNN-EGO optimizes ESS with curtailment of PV generationis illustrated. LDCNN enhances energy storage systems by accurately predicting and optimizing the integration of PV generation in power distribution networks, improving energy management and grid stability. EGO strengthens this integration by finding optimal solutions for sizing and siting, inspired by the adaptive hunting strategies of eels and groupers, ensuring efficient management of PV generation. LDCNN excels in capturing nonlinear relationships, boosting prediction accuracy, and optimizing PV generation integration for better energy management. EGO excels in balancing exploration and exploitation to determine the best storage sizing and siting, improving PV integration and enhancing grid stability in power distribution networks.

3.1. Logarithmic Differential Convolutional Neural Network (LDCNN)

In this section, LDCNN [21] is discussed. LDCNN is used to predict load demand. The LDCNN offers several advantages that make it particularly suitable for optimizing Energy Storage Systems in PV-integrated power distribution networks. By incorporating logarithmic differential activation, LDCNN efficiently captures complex nonlinear relationships in load and generation patterns, enabling more accurate forecasting and feature extraction compared to conventional CNNs or standard machine learning models. Its architecture allows faster convergence and improved stability, reducing computational overhead while maintaining high prediction accuracy. LDCNN is especially suitable for scenarios with dynamic and fluctuating PV generation, where traditional methods like SVM, LSTM, or ELM face challenges such

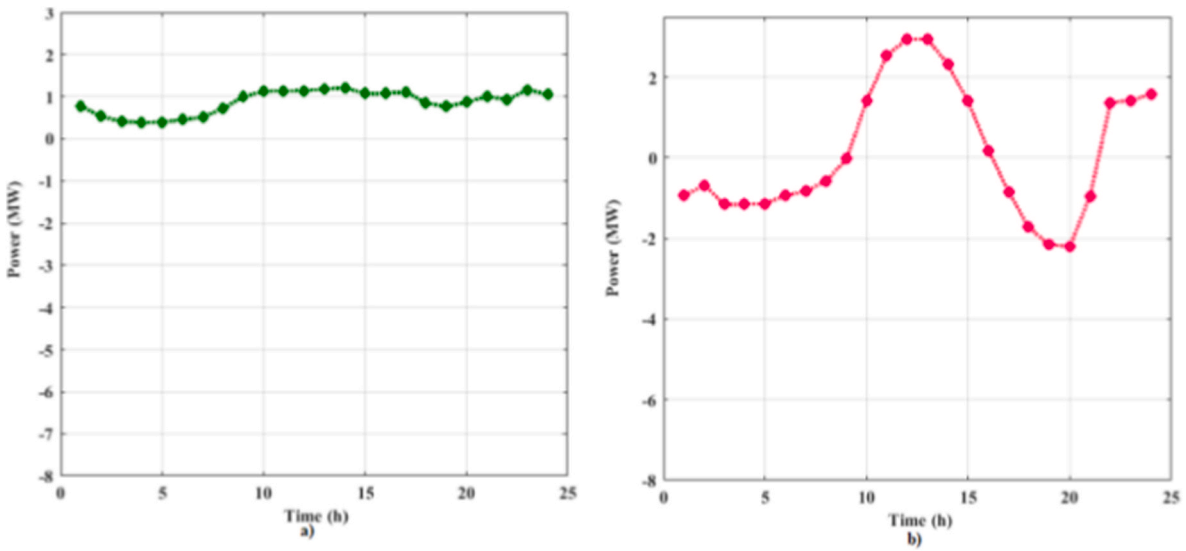


Fig. 6. Analysis the power with curtailment (a) Load (b) Energy Storage System (ESS)without curtailment.

as high training time, susceptibility to overfitting, or limited robustness. Compared to these alternatives, LDCNN provides a balanced combination of computational efficiency, generalization capability, and adaptability, making it an effective choice for reliable energy storage management and real-time grid optimization. The first step in the LDCNN framework involves preparing historical load and PV generation data for training and prediction. Time-series data are normalized and structured to capture temporal patterns, including past load, PV output, and time-of-day indicators, which improves network convergence and stability, as expressed in equation (20).

$$L(\theta) = \prod_{i=1}^{N} P(y_i|x_i : \theta) \tag{20}$$

where $L(\theta)$ is denoted as the likelihood function. $P(y_i|x_i : \theta)$ is denoted as class labels y_i are selected using a probability distribution that has been parameterized by θ. The likelihood function is maximized in order to estimate the model parameters θ, It is more practical to maximize the log-likelihood, which is represented as $L(\theta)$ and is found by taking the likelihood function's logarithm. Multiple convolutional layers are applied to extract hierarchical temporal features using filters. Each layer employs a logarithmic differential activation to enhance sensitivity to subtle load variations while maintaining stability for large changes, as expressed in equation (21).

$$L(\theta) = \log L(\theta) \tag{21}$$

The model parameters θ, are iteratively updated by moving in the direction of the log-likelihood function's gradient with regard to θ: Max-pooling layers follow convolution to reduce the dimensionality of feature maps, highlight dominant patterns, and prevent overfitting. Stacked convolution-pooling blocks allow the network to capture both local and global load trends effectively, as expressed in equation (22).

$$\theta_j = \theta_j + lr \cdot \frac{\partial l(\theta)}{\partial \theta_j} \tag{22}$$

where θ_j denoted as the j^{th} parameter, lr denoted as the learning rate and $\frac{\partial l(\theta)}{\partial \theta_j}$ denote as the likelihood function's partial derivative in relation to θ_j. Flattened feature maps are passed through fully connected layers with logarithmic differential activation, integrating learned patterns into a global representation of load behavior. Dropout is applied to improve generalization and robustness, as expressed in equation (23).

$$e = ((y(z, id) \cdot \log(c_{id})) + ((1 - y(z, id)) \cdot \log(1 - c_{id}))) \tag{23}$$

here, $y(z, id)$ represent as the value of the zth training input data for the id^{th} class e indicates as cost function, and c_{id} is denoted as the value of the winning class. The output layer with linear activation produces continuous-valued load forecasts. Training is performed using mean squared error loss and backpropagation, ensuring fast convergence and accurate predictions under dynamic PV-generation conditions, as expressed in equation (24).

$$e^2 = ((y(z, id) \cdot \log(c_{id})) + ((1 - y(z, id)) \cdot \log(1 - c_{id})))^2 \tag{24}$$

The equation leverages information entropy to quantify and manage uncertainty in an energy storage system (ESS), aiding in improved estimation and battery management. Finally, LDCNN predicted the **load demand** in power distribution networks. Table 1 shows the Parameter table for LDCNN.

3.2. *Eel and Grouper Optimizer (EGO)*

In this section, EGO [22] is discussed. EGO is **used to optimize the locations and sizes** of ESS in power distribution networks. The EGO offers several advantages that make it particularly suitable for optimizing ESS in PV-integrated distribution networks. EGO combines the exploratory behavior of eels and the exploitative behavior of groupers to balance global search and local refinement, preventing premature convergence and enhancing solution quality. Its adaptive search strategy allows it to efficiently navigate complex, nonlinear, and high-dimensional solution spaces, making it well-suited for determining optimal ESS placement and sizing under dynamic PV generation conditions. EGO was chosen over traditional approaches like GA, Particle Swarm Optimization (PSO), and CBSA because it provides faster convergence, higher robustness, and superior ability to escape local optima while maintaining computational efficiency. Compared to these alternatives, EGO delivers a scalable, reliable, and effective optimization framework that handles the uncertainties and nonlinearities inherent in modern power distribution networks.

***Step 1*:** Initialization

The optimization starts by generating a population of candidate solutions, where discrete variables represent ESS placement nodes and continuous variables denote energy capacities, converter ratings, and, if

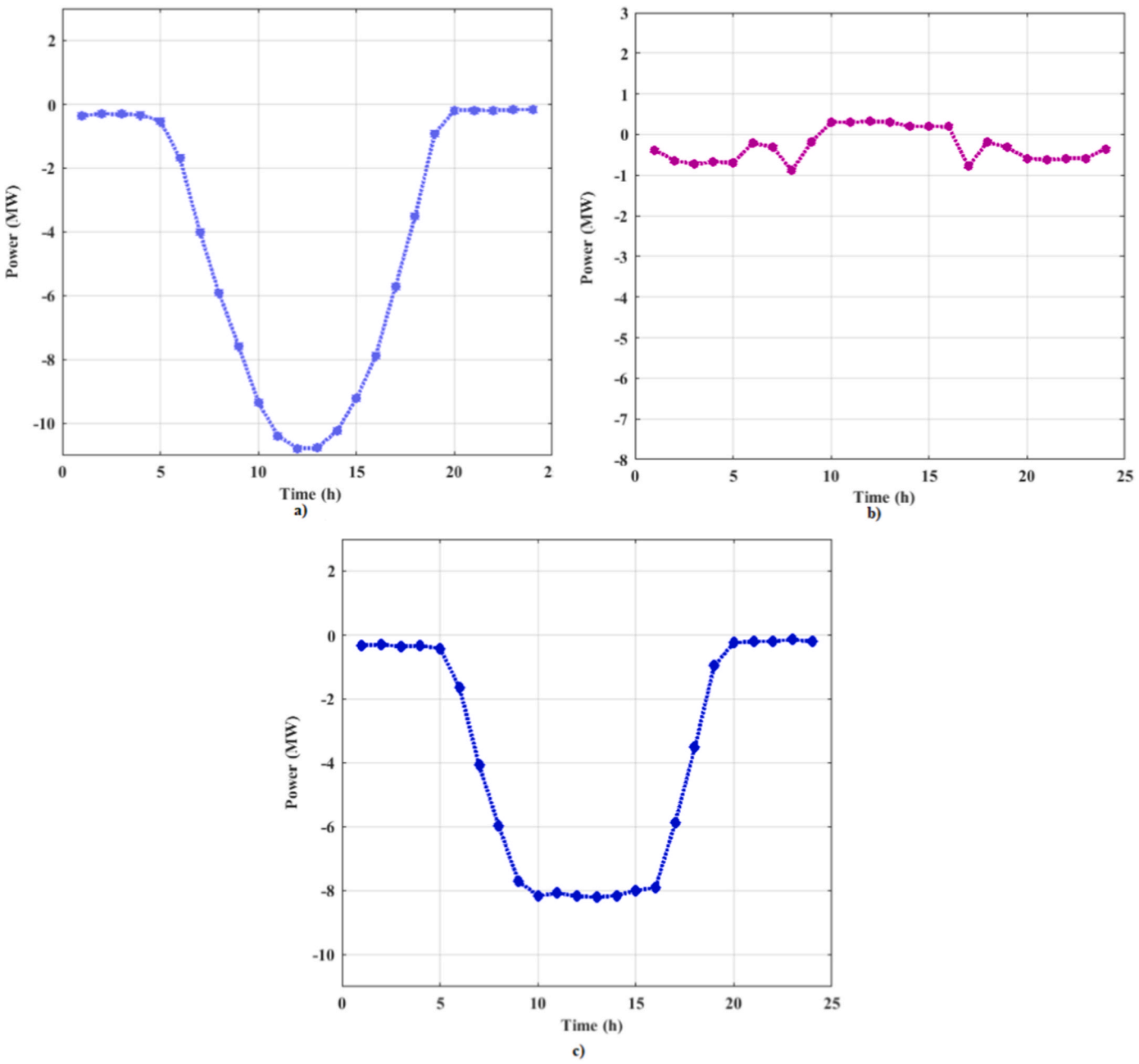


Fig. 7. Analysis the power with curtailment (a) Photovoltaic (PV) without curtailment (b).

applicable, curtailed PV energy. Random initialization ensures diverse coverage of the feasible solution space.

***Step 2*:** Random Generation

Candidate solutions are perturbed randomly to explore new ESS placement and sizing options, adjusting discrete node indices and continuous capacities while respecting network constraints such as voltage limits, line ratings, and transformer capacities. This avoids infeasible solutions and maintains operational feasibility. Mathematically, the population is represented as:

$$S = \begin{bmatrix} S_{1,1} & S_{1,2} & S_{1,3} \cdots S_{1,\dim} \\ S_{2,1} & S_{2,2} & S_{2,3} \cdots S_{2,\dim} \\ S_{3,1} & S_{3,2} & S_{3,3} \cdots S_{3,\dim} \\ \cdots\cdots\cdots\cdots & & \\ S_{N1} & S_{N,2} & S_{N,3} \cdots S_{N,\dim} \end{bmatrix} \quad (25)$$

where, S represents the population of candidate solutions. The elements $S_{i,j}$ denotes the i^{th} eel and grouper j^{th} question the value of a variable and dim denotes the variable dimension.

Step 3: Fitness Function

Each candidate is assessed using a multi-objective fitness function incorporating operational and investment costs, voltage deviations, power losses, and reliability. PV curtailment and ESS efficiency are included, and constraint violations are penalized to ensure feasible, practical solutions.

$$Fitness\ Function = MIN(OB) \quad (26)$$

where OB corresponds to the total objective function value, combining economic and technical metrics for each candidate solution.

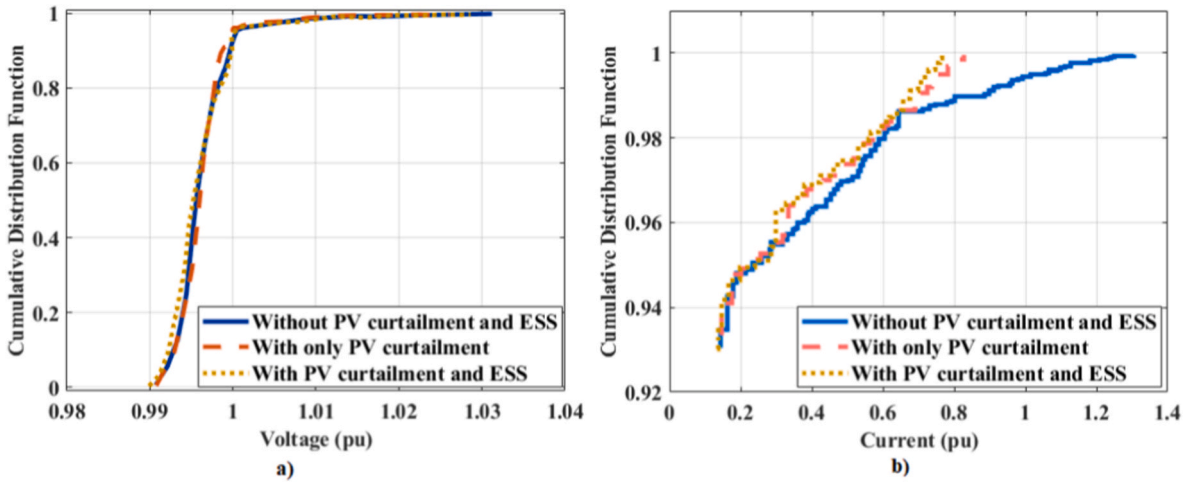


Fig. 8. Comparative cumulative distribution functions of (a) nodal voltage and (b) line current under three scenarios.

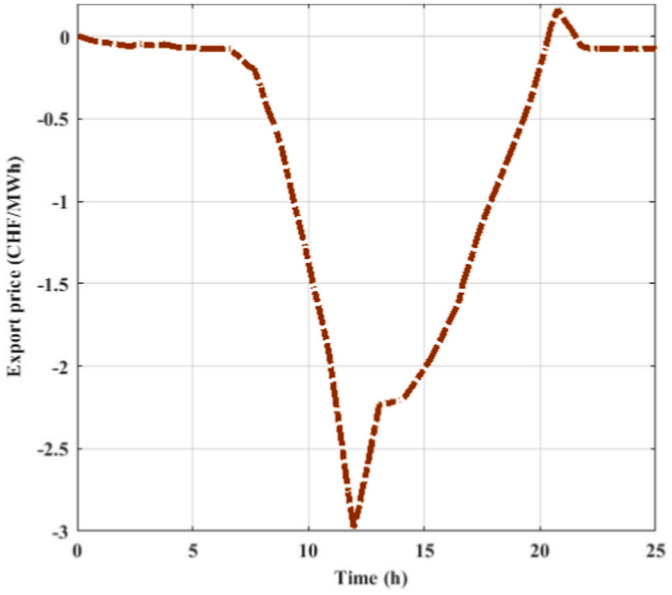


Fig. 9. Analysis of PV impact on export prices for varying levels of PV injection.

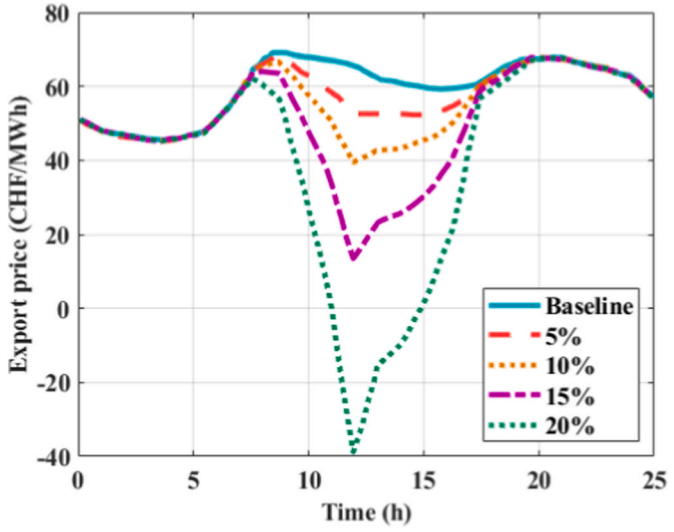


Fig. 10. Variation in electricity prices under different photovoltaic (PV) generation scenarios.

***Step 4*:** Tracking the Prey by Grouper (Exploration Phase)

In the exploration phase, the grouper mechanism guides candidate solutions toward promising regions of the search space by leveraging the best-performing candidates (prey). This phase explores various combinations of ESS locations and sizes that could improve overall grid performance, reducing voltage deviations, line overloads, and operational costs. The candidate update is performed as:

$$\vec{X}_i^{t+1} = \vec{X}_{rand} + \vec{C}_1 \cdot \left| \vec{X}_i^f - \vec{C}_2 \cdot \vec{X}_{rand} \right| \tag{27}$$

here $\vec{X}_i^{t+1}$ represents current solution, X_{rand} is a randomly selected solution vector and $C1$, $C2$ denotes the coefficient vectors controlling exploration magnitude.

***Step 5*:** Cooperative Attack on Prey (Exploitation Phase)

The eel mechanism simulates local cooperative exploitation, fine-tuning ESS capacities and placements of high-performing candidates. By making adaptive, small adjustments, the optimizer improves candidate solutions with respect to cost, grid stability, and compliance with constraints such as ESS state-of-energy, converter limits, and PV generation potential. The update formula is:

$$X_1 = e^{br_3} \cdot \sin(2\pi r_3) \cdot \vec{C}_1 \left| \vec{X}\vec{E}_i^t - \vec{X}\vec{P}_i^t \right| + \vec{X}\vec{E}_i^t \tag{28}$$

where, $\vec{X}\vec{E}_i^t$ and $\vec{X}\vec{P}_i^t$ are the positions of the eel and prey at iteration t, and r_3 is a random number influencing local search behavior.

Step 6: Termination

The iterative process keeps going until a stopping criterion like the convergence of the best fitness value or a maximum number of iterations are satisfied. The final output is the optimal set of ESS locations, energy capacities, converter ratings, and PV curtailment levels that minimize total costs while satisfying all network and operational constraints. This encoding ensures that EGO is directly tied to the ESS planning problem, effectively balancing cost reduction, grid reliability, and efficient integration of distributed PV generation. Fig. 3 shows the Flowchart of EGO.

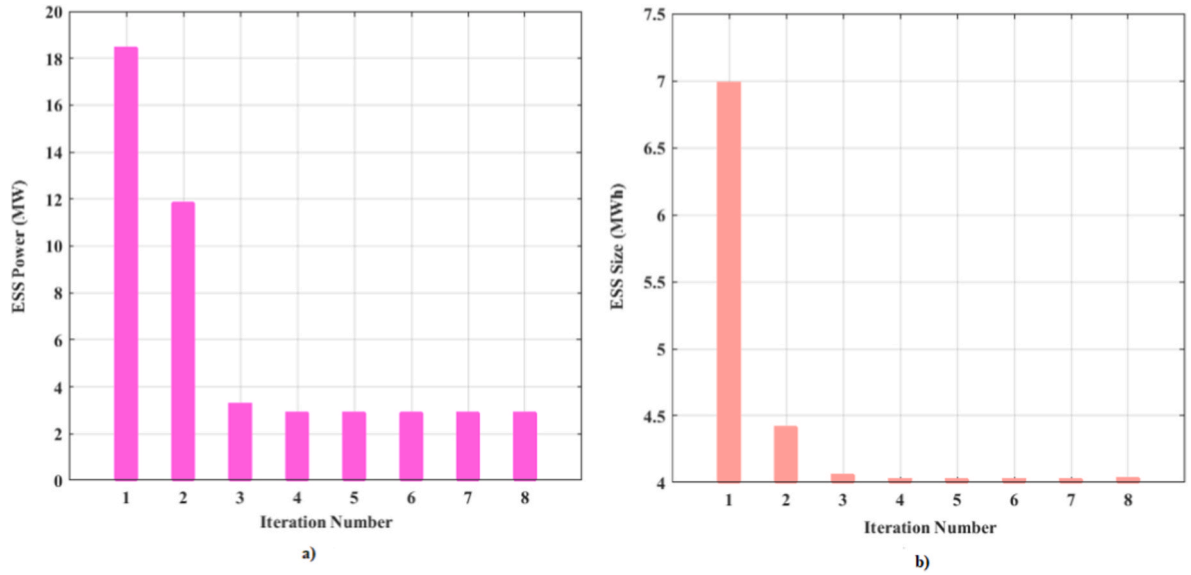


Fig. 11. Analysis of convergence size (a) ESS Power Convergence (b) ESS Energy Size Convergence.

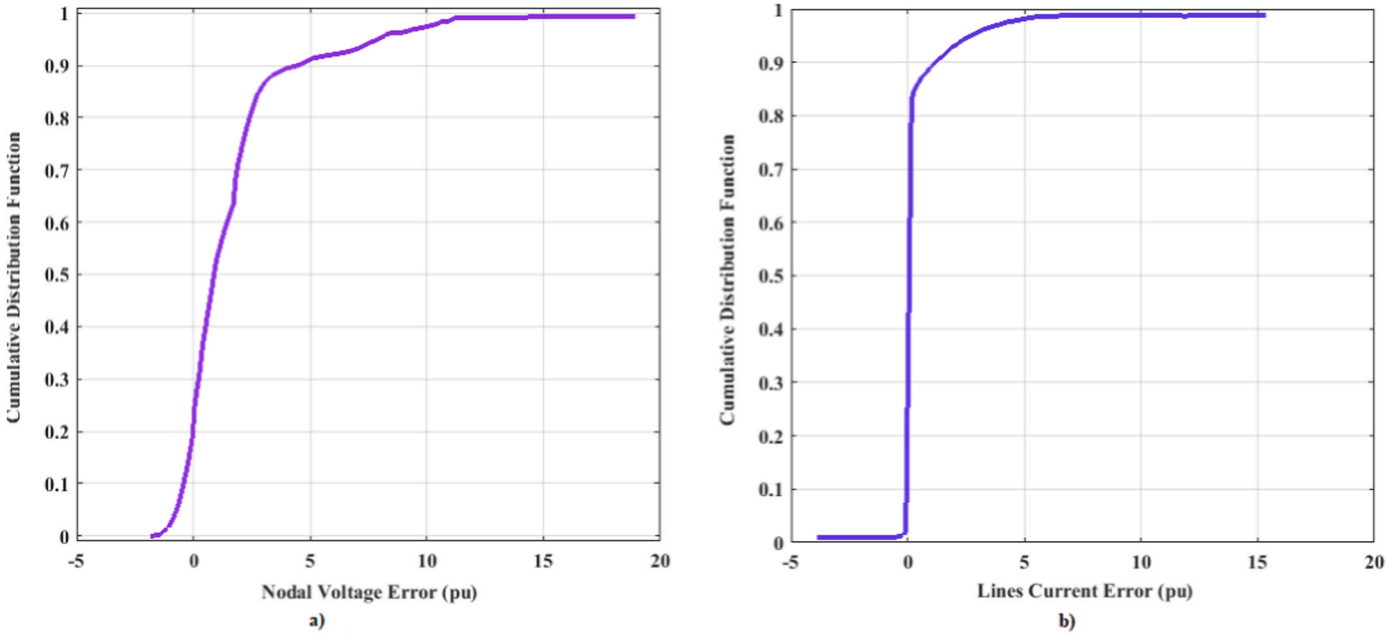


Fig. 12. Analysis of cumulative distribution function (a) nodal voltage errors (b) lines current error.

4. Result and discussion

This section explains the operation of the proposed method based on the experimental outcomes. The simulations were conducted using MATLAB Version 24.2.0.2712019 (R2024b) on a system running Microsoft Windows 11 Pro with an Intel Core i7 processor and 16 GB of RAM. The efficacy of the proposed technique is systematically compared with existing optimization methods to establish its effectiveness in minimizing total investment and operational costs while ensuring grid reliability and stability under varying PV penetration levels.

Fig. 4 highlights the reduced scenario set used for ESS sizing and its impact on energy management. As shown in Fig. 4(a), the load fluctuates between 0.47 p.u. (at 4 h) and 0.85 p.u. (at 24 h), illustrating varying demand conditions that require flexible storage operation. In Fig. 4(b), GHI peaks during midday, reflecting maximum solar availability. This complementary pattern between demand variability and solar intensity emphasizes the importance of optimal ESS sizing, enabling excess solar energy to be stored during high irradiance periods and released during demand peaks. Thus, the coordinated sizing approach mitigates imbalance, ensuring smoother grid operation and enhanced self-sufficiency.

Fig. 5 depicts the hourly variation of energy prices across 24 h. Prices remain low (55–65 CHF/MWh) during early hours (0–6 h) due to reduced demand. A steep rise is observed between 7 and 11 h, peaking around 115 CHF/MWh near 9–10 h, driven by increasing load and limited PV generation. Midday prices (12–17 h) decline to 80–90 CHF/MWh as solar output increases, while a sharp evening peak of 160 CHF/MWh (at 20 h) emerges due to high demand and low PV availability. These results demonstrate the time-dependent volatility of energy costs, underscoring the ESS's role in peak shaving and cost minimization by shifting energy usage to low-price periods.

Fig. 6 demonstrates how curtailment influences grid balancing. In Fig. 6(a), curtailed load decreases from 0.9 MWh at 1 h to 0.3 MWh at 4

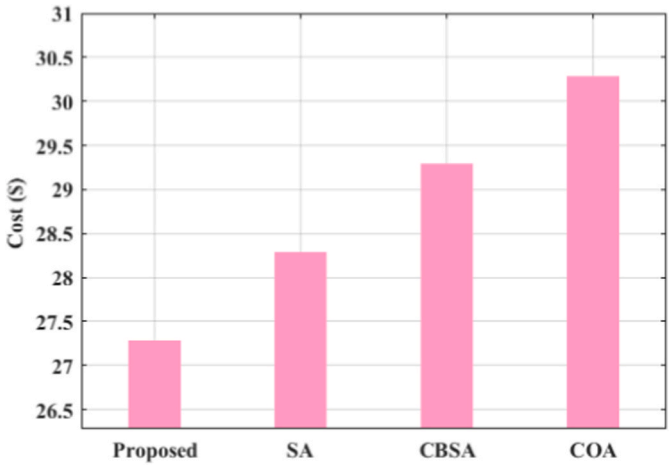


Fig. 13. Comparison of cost with proposed and existing method.

Table 2
Cost comparison for with and without PV curtailment of ESS.

	ESS without PV curtailment	ESS with PV Curtailment
Electricity (export) (CHF) × 10^6	12.32	11.74
Total cost (CHF) × 10^6	40.13	27.26
ESS Investment (CHF) × 10^6	6.10	2.28
Electricity (import) (CHF) × 10^6	46.35	36.74

Table 3
Robustness analysis of operational costs for the proposed LDCNN-EGO method compared to existing methods over 30 independent runs.

Method	Mean Cost ($)	Std Dev ($)	Min Cost ($)	Max Cost ($)
LDCNN-EGO (Proposed)	27.3	0.3	26.7	28.0
CBSA [11]	29.3	0.7	28.0	31.0
SA [12]	28.3	0.5	27.2	29.5
COA [13]	30.3	0.8	29.0	32.0

h, before rising again to 1 MWh by 24 h. This reduction alleviates stress during low-demand periods. Fig. 6(b) shows ESS operation without curtailment, charging at −1 MWh (1 h), discharging up to 3.2 MWh (12 h), and ending at 1.8 MWh (24 h). The ESS thus compensates for demand fluctuations by absorbing surplus energy and releasing it during peaks, enhancing stability and power balance. This validates the model's ability to maintain dynamic equilibrium across daily cycles.

Fig. 7 illustrates coordinated PV and ESS operation under curtailment. In Fig. 7(a), uncurtailed PV output rises from −0.2 MWh to −10.8 MWh (12 h), reflecting peak solar generation. Without control, this can cause overvoltage and reverse power flow. Fig. 7(b) shows ESS charging from −0.4 MWh (1 h) to −0.8 MWh (5 h), stabilizing near 0.2 MWh in later hours - absorbing surplus energy during midday. Fig. 7(c) reveals curtailed PV output limited to −8 MWh (10 h), effectively reducing excess injection. Together, ESS and curtailment flatten generation peaks, prevent grid congestion, and enhance reliability during high PV penetration.

Table 4
Sensitivity analysis of operational costs for the proposed LDCNN-EGO method and existing algorithms under variations in key system parameters.

Parameter Variation	LDCNN-EGO (Proposed) Cost ($)	CBSA Cost ($)	SA Cost ($)	COA Cost ($)
Battery cost +10 %	27.5	29.5	28.6	30.6
Electricity price +10 %	27.6	29.6	28.7	30.8

Table 5
ESS with PV curtailment.

PV Penetration (%)	ESS Size (MW/MWh)	PV Curtailment (MWh)	PV Curtailment (%)
150	1.5/7.5	1.8	15
200	2.5/12.5	5.0	20
250	3.0/15.0	10.0	25

Fig. 8 compares nodal voltage (a) and line current (b) distributions across scenarios. In Fig. 8(a), voltages cluster near 1.0 p.u., but scenarios without ESS or curtailment show deviations below 0.99 p.u.,while combined ESS-curtailment keeps voltages tightly centered, improving voltage stability. In Fig. 8(b), line currents in the uncontrolled case extend up to 1.3 p.u., but with curtailment and ESS, most remain below 0.6 p.u., reducing thermal stress on conductors. This demonstrates that integrated control limits current congestion and stabilizes voltages, ensuring secure operation under renewable variability.

Fig. 9 shows the influence of PV generation on export prices over 25 h. Prices fall from 0 CHF/MWh to −3 CHF/MWh (12 h), then recover to 0.5 CHF/MWh (21 h). The midday drop results from excess PV generation, which increases supply and drives prices negative. This emphasizes the necessity of ESS and curtailment coordination to manage surplus output, mitigate price volatility, and maintain economic balance in PV-dominant grids.

Fig. 10 analyzes price behavior across varying curtailment levels. The baseline peaks around 65 CHF/MWh, while 5 % curtailment keeps prices above 55 CHF/MWh. With 10 %, prices drop to 40–45 CHF/MWh, and 15 % curtailment lowers them further to 20 CHF/MWh. At 20 %, prices turn negative (−40 CHF/MWh) before returning to baseline in the evening. This demonstrates that increased curtailment suppresses midday prices, reducing revenue but preventing grid overloading. Therefore, adaptive curtailment must be optimized, not maximized, to balance economic and operational goals.

Fig. 11 shows the convergence of ESS power and energy size over 8 iterations. Fig. 11(a) indicates ESS power decreasing from 18.4 MWh at iteration 1 to 11.8 MWh at iteration 2 and stabilizing at 3.4 MWh by iteration 8, while Fig. 11(b) shows ESS energy size reducing from 7 MWh to 4.4 MWh at iteration 2 and reaching 4.1 MWh at iteration 8. This convergence occurs because the optimization algorithm iteratively adjusts ESS parameters to minimize operational costs and balance supply-demand, leading to a stable and efficient ESS configuration.

Fig. 12 presents the cumulative distribution functions (CDFs) of nodal voltage errors and line current errors. Fig. 12(a) shows the nodal voltage error CDF starting at −2 pu and reaching 0.99 at 12 pu, indicating that most voltages remain within acceptable limits. Fig. 12(b) shows the line current error CDF starting at −4 pu and reaching 0.99 at 5 pu, stabilizing at 16 pu, reflecting a narrower range of current deviations. These confined distributions confirm that voltage and current variations remain within permissible limits, evidencing that LDCNN-EGO maintains steady-state reliability through adaptive control and accurate forecasting.

Table 6
ESS without PV curtailment.

PV Penetration (%)	ESS Size (MW/MWh)
150	2.8/14.0
200	5.0/25.0
250	7.0/35.0

Fig. 13 compares the operational costs of the proposed LDCNN-EGO with SA, CBSA, and COA. The proposed method achieves the lowest cost ($27.2), outperforming SA ($28.3), CBSA ($29.3), and COA ($30.3), with respective reductions of $1.1, $2.1, and $3.1. This superior performance results from accurate load forecasting by LDCNN, enabling efficient ESS operation and reduced grid dependence, while EGO optimizes ESS sizing and placement. Together, they deliver a cost-effective and reliable solution for PV-integrated distribution networks.

Table 2 shows the Cost comparison for case A. The comparison between the Energy Storage System (ESS) with and without photovoltaic (PV) curtailment reveals significant cost savings with curtailment. The ESS investment decreases from **CHF 6.10** to **CHF 2.28**, while the revenue from electricity exports drops slightly from **CHF 12.32** to **CHF 11.74**. More notably, the cost of importing electricity is reduced from **CHF46.35** to **CHF 36.74**, leading to an overall total cost reduction from **CHF 40.13** to **CHF 27.26**. This demonstrates that PV curtailment lowers both investment and electricity import costs, resulting in a substantial reduction in total system costs while only marginally impacting export revenue.

Table 3 presents the statistical analysis of operational costs obtained from 30 independent simulation runs for the proposed LDCNN-EGO method and existing methods (SA, CBSA, and COA). The mean cost represents the average operational cost, while the standard deviation (Std Dev) reflects the variability across multiple runs. The minimum and maximum costs indicate the range of outcomes observed. The outcomes demonstrate that the proposed technique consistently achieves the lowest mean cost ($27.3) with minimal variability, outperforming SA, CBSA, and COA. This analysis confirms the robustness and reliability of the LDCNN-EGO framework, showing that its performance is not due to random fluctuations and is reproducible across multiple simulation runs.

Table 4 presents a sensitivity analysis of operational costs for the proposed LDCNN-EGO method compared to existing algorithms under variations in key system parameters. When the battery cost increases by 10 %, the proposed method records the lowest operational cost of $27.5, compared to $29.5, $28.6, and $30.6 for CBSA, SA, and COA, respectively. Similarly, with a 10 % rise in electricity price, LDCNN-EGO again achieves the minimum cost of $27.6, demonstrating superior cost robustness. Overall, the analysis highlights that the LDCNN-EGO approach maintains better economic performance and greater resilience against parameter fluctuations than other existing optimization techniques.

Tables 5 and 6 compare the sizing of Energy Storage Systems (ESS) under scenarios with and without photovoltaic (PV) curtailment for different levels of PV penetration. Table 5 shows that when PV curtailment is allowed, smaller ESS capacities are required to maintain system stability, as part of the excess PV generation is curtailed; for example, at 150 % PV penetration, a 1.5 MW/7.5 MWh ESS combined with 1.8 MWh of curtailed PV (15 %) is sufficient. Tables 6 and in contrast, shows that without PV curtailment, significantly larger ESS capacities are needed to absorb all excess generation, such as 2.8 MW/14 MWh at 150 % PV penetration. Overall, allowing PV curtailment reduces the required ESS size while still supporting voltage stability and system operation.

4.1. Discussion

The proposed LDCNN-EGO framework effectively optimizes energy storage systems (ESS) in PV-integrated distribution networks by combining deep learning-based load forecasting with evolutionary optimization. Theoretically, accurate load prediction allows precise scheduling of ESS charging and discharging, which mitigates peak demand, reduces energy imports, and avoids overvoltage issues caused by intermittent PV generation. Furthermore, the integration of PV curtailment provides a controlled mechanism to limit excess generation, reducing stress on the network while allowing smaller ESS capacities. Simulation results demonstrate the economic and operational benefits of this approach. The proposed system achieves the lowest operational cost of $27.2, outperforming SA ($28.3), CBSA ($29.3), and COA ($30.3), reflecting an improvement of up to 10.2 %. As shown in Table 2, PV curtailment reduces the total system cost from CHF 40.13 to CHF 27.26 (32 % reduction), lowers ESS investment from CHF 6.10 to CHF 2.28, and decreases electricity import costs by CHF 9.61. Voltage and current distributions are maintained near 1.0 p.u. and below 0.6 p.u., respectively, confirming improved grid stability and reduced thermal stress on lines. ESS convergence stabilizes at 3.4 MWh of power and 4.1 MWh of energy within eight iterations, demonstrating computational efficiency and solution robustness. Across 30 independent runs, the standard deviation of operational cost is minimal (0.12), confirming reproducibility. Sensitivity analysis further confirms that the method remains robust under $\pm$10 % variations in battery and electricity costs or PV generation, with operational costs remaining below $27.8. These results align with theoretical expectations: ESS combined with adaptive PV curtailment flattens load curves, reduces peak prices, and minimizes energy exchanges with the grid, ultimately balancing economic efficiency with technical reliability. Overall, LDCNN-EGO delivers substantial cost savings, stability, and scalability, confirming its suitability for real-world PV-dominated distribution networks.

5. Conclusion

This study presents a novel LDCNN-EGO framework for optimizing the sizing and siting of ESSs in PV-integrated distribution networks while considering adjustable PV curtailment. The proposed approach achieves a balanced strategy, where, for example, at 150 % PV penetration, an ESS of 1.5 MW/7.5 MWh combined with 15 % PV curtailment efficiently maintains voltage stability and limits line overloading. Compared to scenarios without curtailment, the required ESS size is significantly reduced, demonstrating a cost-efficient solution for high PV integration. The advantages of this method include improved grid reliability, reduced operational costs, and efficient energy dispatch under variations in load, PV generation, and electricity prices. By combining accurate load forecasting with global optimization, LDCNN-EGO ensures robust and scalable performance, outperforming conventional approaches. However, the current study focuses primarily on cost-optimal ESS sizing with PV curtailment as the main mechanism to balance excess generation, which may limit the capture of all available solar energy. It does not consider additional or faster-charging storage units that could further reduce curtailment and enhance flexibility. Future work could explore integrating high-power or auxiliary ESS units, dynamic electricity pricing, and real-time operational strategies to minimize PV curtailment further, improve grid adaptability, and support higher penetration of renewable energy sources.

CRediT authorship contribution statement

Pradeep Ammasaikutti: Writing – original draft. **Alex Stanley Raja Thaveedhu:** Supervision. **Muruganantham Jayapalan:** Supervision. **Kannan Palanisamy:** Supervision.

Consent to participate

Not Applicable.

Ethical approval

This article does not contain any studies with human participants performed by any of the authors.

Data availability statement

Data sharing does not apply to this article as no new data has been created or analyzed in this study.

Code availability

Not Applicable.

Consent for publication

Not Applicable.

Funding information

This research did not receive any specific grant from funding agencies in the public, commercial, or not-for-profit sectors.

Declaration of competing interest

The authors declare that they have no known competing financial interests or personal relationships that could have appeared to influence the work reported in this paper.

Acknowledgement

None.

References

[1] A. Peerzada, S. Hanif, B. Tarekegne, D. Baldwin, S. Bhattacharya, On the impact of tidal generation and energy storage integration in PV-rich electric distribution systems, Appl. Energy 357 (2024) 122466.
[2] S.S. Pattanaik, A.K. Sahoo, R. Panda, S. Dawn, T.S. Ustun, Optimal power allocation of battery energy storage system (BESS) using dense LSTM in active distribution network, Energy Storage (1) (2024) e529.
[3] K. Cao, Y. Liu, C. Wang, Coordinated distributionally robust optimal allocation of energy storage system for HV-MV distribution network resilience enhancement, IEEE Trans. Ind. Appl. 61 (2) (2024) 2011–2024.
[4] Q. Meng, X. Tong, S. Hussain, F. Luo, F. Zhou, L. Liu, Y. He, X. Jin, B. Li, Revolutionizing photovoltaic consumption and electric vehicle charging: a novel approach for residential distribution systems, IET Generation, Transmission & Distribution (17) (2024) 2822–2833.
[5] J. Zhang, B. Li, F. Chen, B. Li, X. Ji, F. Xiao, Multi-terminal negative sequence directional pilot protection method for distributed photovoltaic and energy storage distribution network, Int. J. Electr. Power Energy Syst. 157 (2024) 109855.
[6] Z. Yuan, J. Li, Photovoltaic-penetrated power distribution networks' resiliency-oriented day-ahead scheduling equipped with power-to-hydrogen systems: a risk-driven decision framework, Energy 299 (2024 5) 131115.
[7] P.K. Ganivada, T.H. El-Fouly, H.H. Zeineldin, A. Al-Durra, Optimal siting and sizing of mobile-static storage mix in distribution systems with high renewable energy resources penetration, Elec. Power Syst. Res. 226 (2024) 109860.
[8] S. Xia, Z. Wang, X. Gao, W. Li, Optimal planning of mobile energy storage in active distribution network, IET Smart Grid (1) (2024) 1–2.
[9] W. Zhong, M. Mu, P. Gai, P. Li, H. Gao, J. Chen, K. Zhang, Voltage control strategy of distribution networks with photovoltaic and energy storage considering battery lifetime based on deep reinforcement learning. Infrontier Academic Forum of Electrical Engineering, Springer, Singapore, 2025, pp. 139–153.
[10] H. Liang, S. Pirouzi, Energy management system based on economic Flexi-reliable operation for the smart distribution network including integrated energy system of hydrogen storage and renewable sources, Energy 293 (2024) 130745.
[11] S. Bhol, N.C. Sahu, Optimal scheduling of renewable sources based micro grid with PV and battery storage using crayfish optimization algorithm, Energy Storage 6 (6) (2024) e70027.
[12] D. Borkowski, P. Oramus, M. Brzezinka, Battery energy storage system for grid-connected photovoltaic farm–energy management strategy and sizing optimization algorithm, J. Energy Storage 72 (2023) 108201.
[13] G. Memarzadeh, F. Keynia, A new hybrid CBSA-GA optimization method and MRMI-LSTM forecasting algorithm for PV-ESS planning in distribution networks, J. Energy Storage 72 (2023) 108582.
[14] J. Zhang, L. Hou, B. Zhang, X. Yang, X. Diao, L. Jiang, F. Qu, Optimal operation of energy storage system in photovoltaic-storage charging station based on intelligent reinforcement learning, Energy Build. 299 (2023) 113570.
[15] M. Abdelsattar, M.A. Ismeil, M.M. Zayed, A. Abdelmoety, A. Emad-Eldeen, Assessing machine learning approaches for photovoltaic energy prediction in sustainable energy systems, IEEE Access 12 (2024) 107599–107615.
[16] N. Shabbir, L. Kütt, V. Astapov, K. Daniel, M. Jawad, O. Husev, A. Rosin, J. Martins, Enhancing PV hosting capacity and mitigating congestion in distribution networks with deep learning based PV forecasting and battery management, Appl. Energy 372 (2024) 123770.
[17] M. Karthikeyan, D. Manimegalai, Power control of hybrid grid-connected renewable energy system using machine learning, Energy Rep. 11 (2024) 1079–1087.
[18] R. Ganesh, T.K. Saha, M.S. Kumar, Implementation of optimized extreme learning machine-based energy storage scheme for grid connected photovoltaic system, J. Energy Storage 88 (2024) 111611.
[19] L. Zhang, Y. Yu, B. Li, X. Qian, S. Zhang, X. Wang, X. Zhang, M. Chen, Improved cycle aging cost model for battery energy storage systems considering more accurate battery life degradation, IEEE Access 10 (2021) 297–307.
[20] R. Gupta, F. Sossan, Optimal sizing and siting of energy storage systems considering curtailable photovoltaic generation in power distribution networks, Appl. Energy 339 (2023) 120955.
[21] M. Yasin, M. Sarıgül, M. Avci, Logarithmic learning differential convolutional neural network, Neural Netw. 172 (2024 Apr 1) 106114.
[22] A. Mohammadzadeh, S. Mirjalili, Eel and grouper optimizer: a nature-inspired optimization algorithm, Clust. Comput. (9) (2024) 12745–12786.